

Deep Transfer Convolutional Neural Network and Extreme Learning Machine for Lung Nodule Diagnosis on CT images

Xufeng Huang^a, Qiang Lei^{b,c}, Tingli Xie^d, Yahui Zhang^e, Zhen Hu^f, Qi Zhou^{a,*}

^a School of Aerospace Engineering, Huazhong University of Science & Technology, Wuhan 430074, PR China

^b Department of Medical Imaging, Guangdong No.2 Provincial People's Hospital, Guangzhou 510317, PR China

^c Department of Radiology, The First Affiliated Hospital of Guangzhou Medical University, Guangzhou 510120, PR China

^d George W. Woodruff School of Mechanical Engineering, Georgia Institute of Technology, Atlanta, GA 30332, USA

^e Informatics Institute, Faculty of Science, University of Amsterdam, Amsterdam, The Netherlands

^f Department of Industrial and Manufacturing Systems Engineering, University of Michigan-Dearborn, Dearborn, MI 48128, USA

Abstract

Diagnosis of benign–malignant nodules in the lung on Computed Tomography (CT) images is critical for determining tumor level and reducing patient mortality. Deep learning-based diagnosis of nodules in lung CT images, however, is time-consuming and less accurate due to redundant structure and the lack of adequate training data. In this paper, a novel diagnosis method based on Deep Transfer Convolutional Neural Network (DTCNN) and Extreme Learning Machine (ELM) is explored, which merges the synergy of two algorithms to deal with benign–malignant nodules classification. An optimal DTCNN is first adopted to extract high-level features of lung nodules, which has been trained with the ImageNet dataset beforehand. After that, an ELM classifier is further developed to classify benign and malignant lung nodules. Two datasets, including the Lung Image Database Consortium and Image Database Resource Initiative (LIDC-IDRI) public dataset and a private dataset from the First Affiliated Hospital of Guangzhou Medical University in China (FAH-GMU), have been conducted to verify the efficiency and effectiveness of the proposed approach. The experimental results show that our novel DTCNN-ELM model provides the most reliable results compared with current state-of-the-art methods.

Keywords: Lung Nodule Diagnosis; Computed Tomography; Convolutional Neural Network; Extreme Learning Machine; Transfer learning

1. Introduction

Lung cancer is the foremost cause of cancer-related death worldwide. Although target therapeutics and various chemotherapy regimens have been adapted for cancer-treating, it is challenging to cure thoroughly for locally advanced lung cancer [1]. The early diagnosis of a lung lesion is recognized as the most important method to increase the likelihood of survival rate. Therefore, it is necessary to develop efficient and accurate lung nodule diagnosis methods for the recognition of the potential malignant tumor.

Recently, pulmonologist started to adopt low-dose chest CT images and Machine Learning (ML) techniques to diagnose lung cancers [2-3]. The traditional algorithmic method for detection based on the CT images analysis contains three steps [4]: (1) Feature extraction: hand-crafted lung nodules segmentation and labeled [5]; (2) Feature recognition: recognition of each segmented lung nodules using ML method, such as Support Vector Machine (SVM) [6-8], Random Forest (RF) [9], Artificial Neural Networks (ANNs) [10] and Local Kernel Regression Models (LKRM)

* Corresponding author. E-mail address: qizhouhust@gmail.com & qizhou@hust.edu.cn

[11]; (3) Diagnosis: diagnosis of the whole CT images according to the characterization (i.e., benign or malignant) of the nodules. Nevertheless, these methods rely heavily on the feature extraction processes, which are not only tedious and time-consuming, but also demanding of costly, specialty-oriented knowledge and skills.

Instead, Deep Learning (DL) provides a promising solution to address the above drawbacks. DL models have a strong capability in obtaining high-level features from input data and building the relationships between input and target with multiple layers [12-13]. Hua et al. [14] adopted the Deep Belief Network (DBN) and a shallow Convolutional Neural Network (CNN) with Multiple Layer Perceptron for the classification of pulmonary nodules. Although the DBN and CNN achieved better performance compared with Scale Invariant Feature Transform (SIFT) and fractal method, the performance of sensitivity and specificity were less than 85% in the Lung Image Database Consortium and Image Database Resource Initiative (LIDC-IDRI) dataset [15-16], which was inadequate for medical applications. A multi-feature fusion deep-learning algorithm for the classification of lung nodules on CT images was introduced [17]. This algorithm developed a gray level co-occurrence matrix-based surface descriptor, a fourier-shape descriptor, and a Deep Convolutional Neural Network (DCNN) to extract the features of nodules. After feature extraction, an ensemble model based on Back Propagation Neural Network (BPNN) and Adaptive Boosting (AdaBoost) was adopted to discriminate malignant from benign nodules. Lakshmanaprabu et al. [18] presented a novel automated lung cancer diagnosis method by combining Optimal Deep Neural Network (ODNN) and Linear Discriminate Analysis (LDA), which optimized by Modified Gravitational Search Algorithm (MGSA). This method fused three features (i.e., histogram features, texture feature, and wavelet features), which were reduced by LDA to decrease the computational burden. Considering the limited sampling data, Xie et al. [19] designed a Semi-Supervised Adversarial Classification (SSAC) model using Semi-Supervised Learning (SSL) and Generative Adversarial Nets (GANs), which can be trained with unlabeled and small labeled data simultaneously. The SSAC model utilized the Multi-View Knowledge-Based Collaborative (MV-KBC) learning mentioned in [17], which achieved the accuracy of 92.53% and the specificity of 96.28% in the LIDC-IDRI database. Similarly, Wang et al. [20] developed an innovative fine-grained classification method for lung nodules in CT images, which used Wasserstein Generative Adversarial Networks (WGANs) for data augmentation of lung nodules and improvement of imbalanced data problem. Nonetheless, since SSL and generative models need redundant iterative solutions and easily fall into local optimum, these methods are still tedious and time-consuming.

Despite the fact that the DCNN-based approaches have superior performance compared with those hand-crafted methods, they have not achieved the satisfactory performance on lung tumor CT images classification compared with what they have done in the ImageNet competition [21-23]. What is more, DCNN-based models may overfit the training data because there are ordinarily small datasets in medical image analysis due to the difficulty of data acquisition and annotation. In the case of benign-malignant lung nodules, the available amount of training examples is limited. For example, the LIDC-IDRI dataset is the largest publicly available dataset propitious for benign-malignant nodules diagnosis research while it only contains a few thousand training samples. To resolve this problem, a pre-trained DTCNN [24-28] has been designed since it has been widely recognized that the image representation ability learned from large-scale datasets (i.e. ImageNet [29]) can be efficiently transferred to generic visual recognition tasks, where the training data is limited [30]. Generally, the later-layers of pre-trained DTCNN are fully-connected layer and softmax layer, which have inferior generalization performance and cannot take full advantage of features extracted by pre-trained layers of DTCNN.

Therefore, this study aims to develop an effective lung tumor diagnosis method to provide an accurate and timely diagnosis of key pathology in each lung CT image. This method is based on DTCNN and ELM, which is suitable for

small dataset problems and has advantages in the improvement of classification accuracy and the reduction of computational costs. The contributions of the current research are summarized below:

- 1) An optimal pre-trained DTCNN using Global Average Pooling (GAP) and transfer learning is adopted to extract high-level features of lung nodules;
- 2) A novel approach based on DTCNN and ELM for diagnosis of benign–malignant nodules is proposed, which could fully utilize the representative features and significantly reduce the computational burden;
- 3) Experimental cases, including the LIDC-IDRI public dataset and FAH-GMU private dataset, are conducted to validate the effectiveness and efficiency of the proposed method.

This paper is divided into five sections. Section 2 introduces the background of CNN and ELM. Section 3 demonstrates the details of the proposed DTCNN-ELM approach. Section 4 presents the experiments and testing results to demonstrate the applicability of the proposed method. The conclusion and future research works are drawn in Section 5.

2. Background

2.1. Convolutional Neural Network

CNN [31] is a variant of a multilayer fully connected feedforward neural networks, which could automatically extract local features to perform classification. Though a lot of variants of the CNN model have been presented, the basic structure of CNN for medical image classification contains Convolutions (Conv) Layer, Pooling Layer (i.e., Subsampling), Dense Layer (i.e., Fully-Connected) and Softmax Layer [14]. Fig. 1 shows the basic structure of CNN for medical image classification.

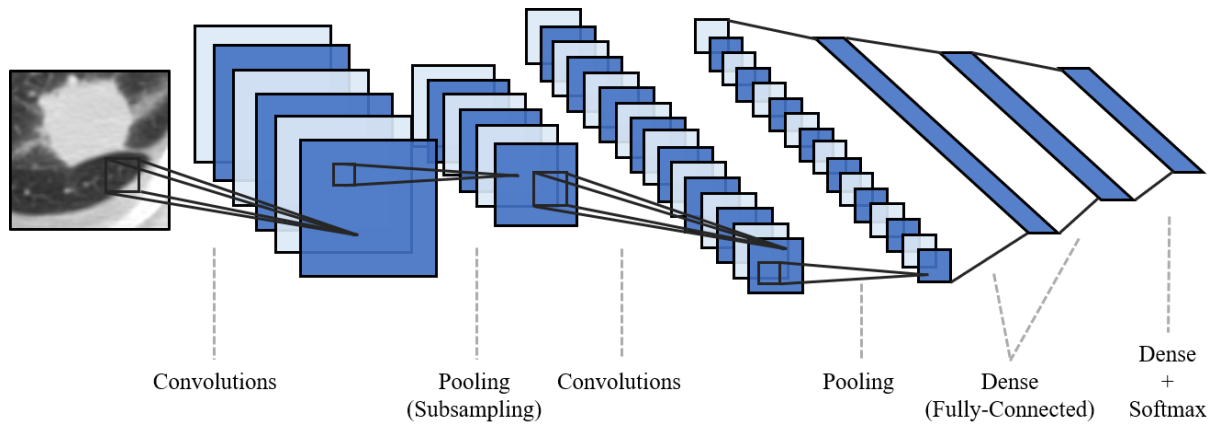


Fig. 1. The basic structure of CNN for medical image classification

The Conv Layer is designed to extract high-level features of the medical image automatically, which using the convolution operation to filter the noise in the original images and enhance the valuable task-related information. The Pooling Layer is typically applied with Conv Layer interchangeably, which is employed for dimension reduction of features parameters and achievement of translation-invariant characteristics (i.e., average pooling and max pooling). The Dense Layer is applied to convert the features from Pooling Layer into 1-D vectors and to realize the classification for different tasks. In Softmax Layer, the representative vectors from Dense Layer are reshaped and mapped into a probability distribution for classification. Eventually, the whole CNN is trained by the Back Propagation (BP) algorithm with a gradient-based optimization algorithm [31]. After training, the parameters (i.e., the weights of the

convolution kernel) of the CNN are adjusted and optimized. Therefore, an optimal CNN is obtained, which can be used for either prediction or classification.

2.2. Extreme Learning Machine

Huang et al. [32-33] firstly proposed ELM for Single-Hidden Layer Feedforward Neural Networks (SLFNs), which can improve the efficiency of the BP algorithm and simplify neural network parameters. Different from ANN, ELM randomly initiates the parameters of hidden layers and determines the output weights according to the minimum norm least squares solution [34]. The basic architecture of ELM is shown in Fig. 2, which contains n input nodes, l hidden nodes and m output nodes. For N learning samples $x_i, y_i \in R^{n \times m}$ $i = 1, 2, \dots, N$, the ELM model can be defined by the following equation:

$$\begin{cases} f(\mathbf{x}_j) = \sum_{i=1}^l \beta_i G_i(\mathbf{x}_j) = \mathbf{G}(\mathbf{x}_j) \boldsymbol{\beta} \\ G_i(\mathbf{x}_j) = g_i(w_i x_j + b_i) \end{cases} \quad j = 1, 2, \dots, n \quad (1)$$

where $\boldsymbol{\beta} = [\beta_1, \beta_2, \dots, \beta_l]^T$ is the matrix of output weights between the output nodes and the hidden nodes, \mathbf{G} expresses the activation function of the hidden layer, w_i is the weight between the input layer and i^{th} hidden layer, and b_i is the i^{th} hidden bias.

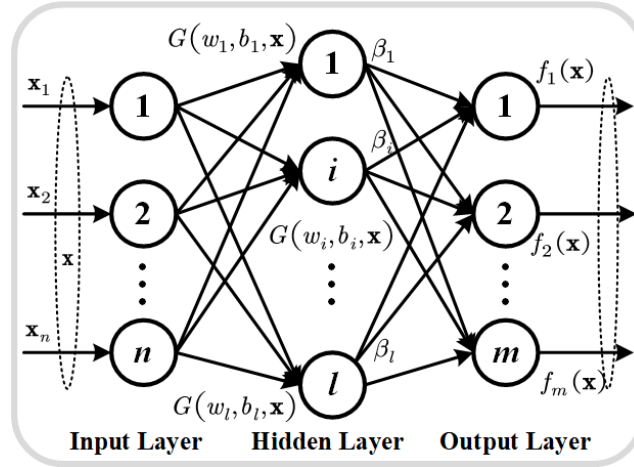


Fig. 2. The basic structure of ELM

Once the weights $\mathbf{w} = [w_1, w_2, \dots, w_l] \in R^{n \times l}$ and the biases $\mathbf{b} = [b_1, b_2, \dots, b_l] \in R^{1 \times l}$ are randomly initiated, the hidden layer nodes \mathbf{H} can be calculated by the following equation:

$$\mathbf{H} = \begin{bmatrix} \mathbf{G} \mathbf{x}_1 \\ \vdots \\ \mathbf{G} \mathbf{x}_n \end{bmatrix} = \begin{bmatrix} g_1 \mathbf{w}_1^T \mathbf{x}_1 + b_1 & g_2 \mathbf{w}_1^T \mathbf{x}_1 + b_2 & \cdots & g_l \mathbf{w}_1^T \mathbf{x}_1 + b_l \\ g_1 \mathbf{w}_1^T \mathbf{x}_2 + b_1 & g_2 \mathbf{w}_1^T \mathbf{x}_2 + b_2 & \cdots & g_l \mathbf{w}_1^T \mathbf{x}_2 + b_l \\ \vdots & \vdots & \ddots & \vdots \\ g_1 \mathbf{w}_1^T \mathbf{x}_n + b_1 & g_2 \mathbf{w}_1^T \mathbf{x}_n + b_2 & \cdots & g_l \mathbf{w}_1^T \mathbf{x}_n + b_l \end{bmatrix} \quad (2)$$

Then, the output weight $\boldsymbol{\beta}$ is calculated by minimizing the squared error regarding the training samples [35]. Therefore, the objective function of ELM can be represented by the following equation:

$$\min_{\mathbf{w}, \mathbf{b}, \boldsymbol{\beta}} \|\mathbf{H} \boldsymbol{\beta} - \mathbf{Y}\| \quad (3)$$

where $\mathbf{Y} = [\mathbf{y}_1, \mathbf{y}_2, \dots, \mathbf{y}_m] \in R^{c \times m}$ is the target matrix of training data, c is the class number in the output layer.

It is easy to solve this optimization problem using a gradient descent-based optimization algorithm (e.g., batch gradient descent (BGD) and stochastic gradient descent (SGD)). However, in ELM, the output matrix of the hidden

layer \mathbf{H} is defined uniquely because of the random weight assignment. Consequently, the optimal solution for β can be expressed by the following equation:

$$\beta = \mathbf{H}^+ \mathbf{Y} \quad (4)$$

where \mathbf{H}^+ is the Moore-Penrose generalized inverse matrix \mathbf{H} .

The whole training process completes at one time without tedious iterations. Eventually, the ELM model obtains the optimal parameters and minimum training errors.

3. The proposed DTCNN-ELM method

In this section, a novel DTCNN-ELM method for lung nodules diagnosis is developed, which can tackle the problems of small data and improve the training speed. As shown in Fig. 3, the proposed method consists of two parts: the preprocessing of lung nodules in CT images and the diagnosis of lung nodules based on the proposed DTCNN-ELM.

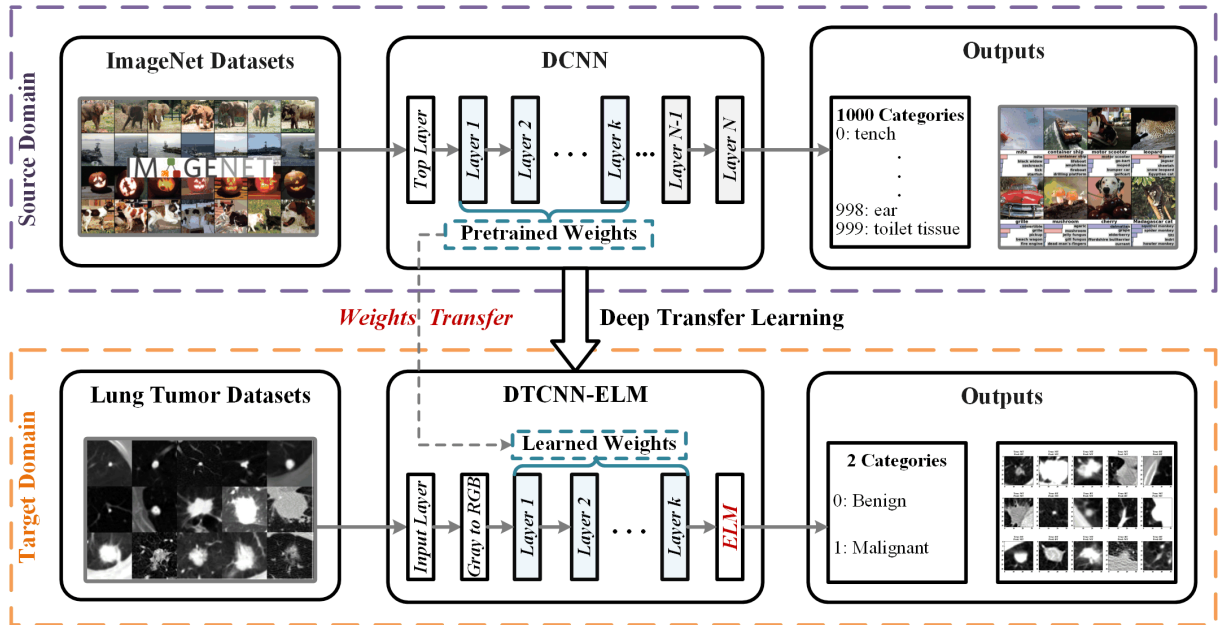


Fig. 3. The Architecture of the proposed DTCNN-ELM method

3.1. Preprocessing of lung nodules in CT images

All nodule Region of Interest (ROI) patches from lung CT images are firstly preprocessed to the dimension of 64×64 using the Zero Padding method. Fig. 4 shows the flowchart of preprocessing for lung nodules.

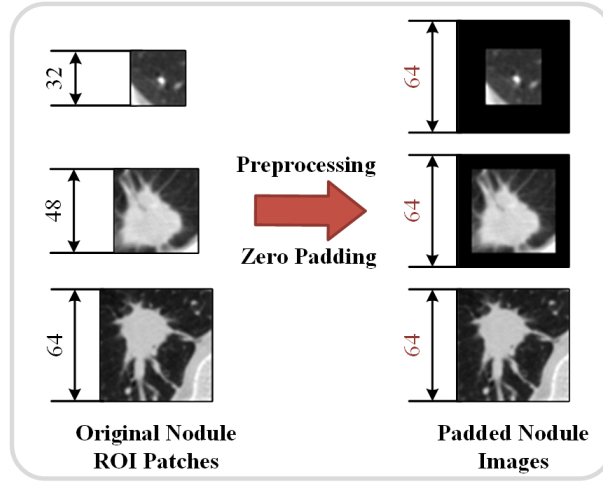


Fig. 4. Preprocessing for lung nodules

Meanwhile, input gray (1-channel) images are converted to RGB (3-channels) images by duplicated three times, which are fitted for the input layer of pre-trained DTCNN. Besides, to reduce the computational costs, no other pre-processing technique is employed in the proposed DTCNN-ELM method.

3.2. Lung nodules diagnosis based on the proposed DTCNN-ELM

After the lung nodules data are successfully preprocessed, a set of 64×64 pixels images are generated. Then, the problem of benign-malignant nodules diagnosis is solved by classifying these images. Due to the insufficient labeled data in medical classification and the time-consuming process of training DCNN, network-based deep transfer learning is used in this paper to improve the efficiency of training CNN model with a limited amount of labeled data [36-37]. Low-level features in the front-layers of CNN are universal for different but related tasks, while high-level features in the later-layers are specific for different tasks. Thus, the front-layers of CNN are always regarded as a universal feature extractor. Based on this remark, an optimized DTCNN is proposed to classify these lung nodule images. The general procedures of the proposed method can be summarized as follows,

- Step.1.** Lung nodules ROI square patches are obtained from lung CT images according to different sizes of nodules.
- Step.2.** The Zero Padding is used to convert different sizes of nodules into the same dimension (i.e., from 32×32 and 48×48 to 64×64) images to obtain useful representative features.
- Step.3.** The DTCNN is constructed, which consists of a pre-trained DCNN model and a target DCNN model, where the pre-trained DCNN model is used to extract universal features for common image classification, and the target DCNN model aims to classify nodules efficiently and accurately with the aid of the pre-trained DCNN. Also, the Global Average Pooling (GAP) [38] is used to replace the dense layers in DTCNN.
- Step.4.** The ELM is constructed, and the parameters are determined, including the number of hidden nodes l . Then, the ELM is combined with the DTCNN and used as a classifier.
- Step.5.** In DTCNN-ELM, the training samples are firstly fed into the DTCNN architecture to obtain the feature maps. Then all the features are combined and regarded as the inputs of the ELM model, which can be efficiently trained by a generalized inverse operation.
- Step.6.** At the testing phase, the testing samples are fed into the trained DTCNN-ELM model to obtain the final diagnosis results.

4. Experimental results and discussion

In this section, two case studies, including the LIDC-IDRI public dataset and FAH-GMU private dataset, are conducted to validate the effectiveness of the proposed DTCNN-ELM method. All experiments were implemented in Python with TensorFlow (Python 3.6.9, TensorFlow 2.0.0) and run on Windows 10 with 32GB RAM, Intel Core i7 processor, and an Nvidia RTX 2080 GPU. Besides, The ELM was implemented using the hpelm 1.0.10 library.

4.1. Evaluation Metrics

To evaluate the performance of the proposed approach, accuracy (Acc), sensitivity (Sen), specificity (Spc), and area under the receiver operator curve (AUC) metrics are used, as shown in Table 1.

Table 1 Evaluation metrics

| Metrics | Calculation Equations |
|-------------------|--|
| Accuracy (Acc) | $Acc = \frac{TP + TN}{TP + TN + FP + FN}$ |
| Sensitivity (Sen) | $Sen = \frac{TP}{TP + FN}$ |
| Specificity (Spc) | $Spc = \frac{TN}{TN + FP}$ |
| AUC | $AUC = \int_0^1 t_{pr}(f_{pr})d f_{pr} = P(x_p > x_n)$ |

where TP , TN , FP , FN represent the number of true positive, true negative, false positive and false negative, respectively. t_{pr} and f_{pr} denote true positive rate and the false positive rate along ROC, and x_p and x_n are the confidence scores for a positive and negative instance, respectively.

4.2. Lung Nodule diagnosis with LIDC-IDRI

4.2.1. LIDC-IDRI dataset description

The LIDC-IDRI [15-16] in The Cancer Imaging Archive (TCIA) is initiated by the National Cancer Institute (NCI) and improved by seven institutions, which contains a total of 1,012 clinical chest CT scans with more than 200,000 slices images of size $512 \times 512 \times 1$. The scans were acquired in different tube peak potential energies (e.g., 120 kV, 130 kV, 135 kV, and 140 kV) with 40 to 627 mA. Each scan was annotated by at least three experienced radiologists and had a correlated XML file with the details of the malignancy and locations of nodules. In this study, we only extracted the nodules range from 3 mm to 30 mm according to marks in the XML files because smaller nodules (diameter less than 3 mm) are slighter clinically relevant by several nodules screening schemes [7, 19]. Therefore, 2,757 nodules were cropped into different pixel (i.e., $32 \times 32 \times 1$ or $48 \times 48 \times 1$) and annotated with benign and malignant. Fig. 5 shows the raw examples of benign and malignant nodules from the LIDC-IDRI dataset.

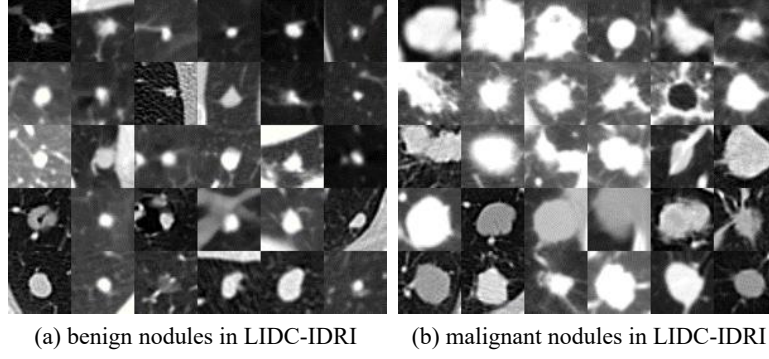


Fig. 5. Raw examples of (a) benign nodules and (b) malignant nodules in the LIDC-IDRI dataset.

4.2.2. LIDC-IDRI Training Details

During the training process, Adam is applied for optimization with batches of size 64. The initial learning rate is set as 0.01 and decreases every 4 epochs with the factor of learning rate decay 0.5. The total number of training epoch is set as 25 in our experiments. Unless otherwise stated, all experiments are conducted 5 times in 5-fold cross-validation to avoid contingency in the testing process and the average values are considered as the final classification results for analysis.

4.2.3. The effectiveness of optimal DTCNN on LIDC-IDRI

The optimal DTCNN structure needs to be selected for the LIDC-IDRI database. Therefore, the experiments of classification were run on different DTCNN architectures (i.e., ResNet50, Xception, NASNetMobile, MobileNetV2, EfficientNet-B5) by applying Softmax classifier.

Table 2 Classification performance for different DTCNN on LIDC-IDRI

| No. | DTCNN | Results (%) (Mean) | | | |
|-----|-----------------|--------------------|--------------|--------------|--------------|
| | | Acc | Sen | Spc | AUC |
| 1 | ResNet50 | 86.23 | 98.20 | 78.18 | 88.19 |
| 2 | Xception | 92.39 | 93.69 | 91.52 | 92.60 |
| 3 | NASNetMobile | 87.68 | 74.77 | 96.36 | 85.57 |
| 4 | MobileNetV2 | 82.97 | 69.37 | 92.12 | 80.75 |
| 5 | EfficientNet-B5 | 88.77 | 94.59 | 84.85 | 89.72 |

The results (mean values) of the five DTCNN methods are shown in Table 2. The highest value of Sensitivity is from ResNet50, achieving an Acc of 86.23%, a Sen of 98.20%, a Spc of 78.18%, an AUC of 88.19%. Additionally, the highest value of Spc is from NASNetMobile, achieving an Acc of 87.68%, a Sen of 74.77%, a Spc of 96.36%, an AUC of 85.57%. Although the ResNet50 and NASNetMobile have achieved higher Sen and Spc, respectively, they are not the optimal structure due to inferior metric values of Acc and AUC. It can be seen that the highest values of Acc and AUC are from Xception, achieving a Sen of 93.69% and a Spc of 91.52%. Thus, Xception is the optimal DTCNN structure used for feature extractor in the LIDC-IDRI dataset.

4.2.4. The efficiency of ELM on LIDC-IDRI

To verify the efficiency of the ELM classifier, two typical classifiers applied in DL-based lung nodules diagnosis, SVM and Softmax, are used for comparison in this experiment. These classifiers are both combined with the Xception

feature extractor. SVM is adopted to conduct the two-category or multiclass classification, requiring the selection of only one parameter, i.e., the regularization term C . In the experiment, C is optimally selected as 0.5 by using a grid search scheme in a massive value range of $\{0.0005, 0.005, 0.05, 0.5, 5\}$. For the Softmax, the Adam algorithm is employed to optimize the weights with 25 epochs. The number of hidden nodes l in ELM is set as 500. The classification results and the computational costs are listed in Table 3.

Table 3 Classification results and computational costs of different classifiers on the LIDC-IDRI dataset.

| Classifiers | Results (Mean) | | | | | |
|-------------|----------------|--------------|--------------|--------------|-------------------|------------------|
| | Acc (%) | Sen (%) | Spc (%) | AUC (%) | Training Time (s) | Testing Time (s) |
| SVM | 91.68 | 88.38 | 91.39 | 91.89 | 2.89 | 0.87 |
| Softmax | 92.39 | 89.19 | 94.55 | 92.32 | 90.62 | 0.74 |
| ELM | 94.57 | 93.69 | 95.15 | 94.94 | 1.72 | 0.12 |

From the results in Table 3, it can be seen that the ELM classifier has the best performance, achieving an Acc of 94.57%, a Sen of 93.69%, a Spc of 95.15%, and an AUC of 94.94%. Moreover, ELM achieves great superiority in computational speed compared with the other two classifiers. When combined with Xception, the training time of ELM is only 1.72s, while those of SVM and Softmax are 2.89s and 90.62s, respectively. Thus, ELM shows equal advantages to the Softmax and outperforms the SVM in training time. Furthermore, the testing time of ELM is less than those of SVM and Softmax. It takes only 0.12s to predict for all the 276 testing samples, which will be beneficial for the real-time diagnosis task.

4.2.5. Comparison to the state-of-the-art methods on LIDC-IDRI

The classification results of state-of-the-art methods are listed in Table 4. As referred in Table 4, the proposed DTCNN-ELM method has the best performance, with an Acc of 94.57%, a Sen of 93.69%, a Spc of 95.15%, and an AUC of 94.94%. In addition, the proposed DTCNN-ELM method is up to 1000 times faster than the approach mentioned in [19] for the classification of each nodule. It shows that the DTCNN-ELM algorithm outperforms the state-of-the-art methods in term of both generalization performances and computational costs.

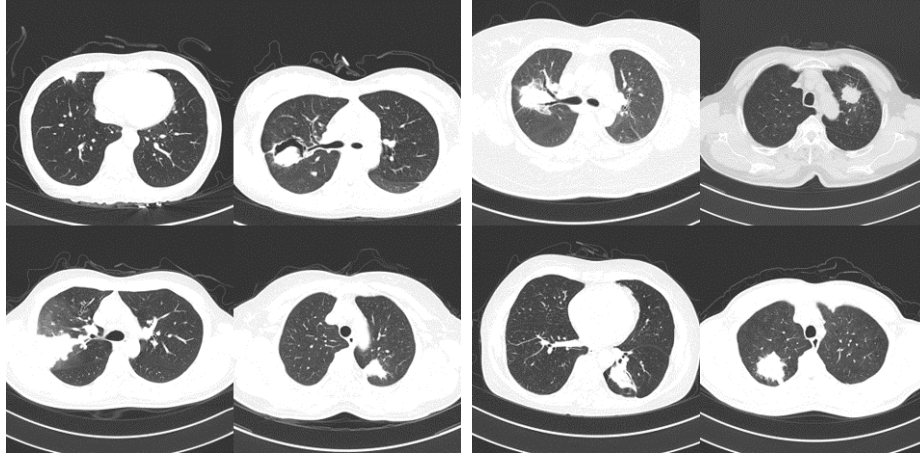
Table 4 Classification results of different state-of-the-art methods on the LIDC-IDRI dataset.

| Methods | Samples | Results (Mean) | | | | | |
|------------------------|--------------|----------------|--------------|--------------|--------------|-------------------|------------------------------|
| | | Acc (%) | Sen (%) | Spc (%) | AUC (%) | Training Time (s) | Testing Time per nodule (ms) |
| Chen et al., 2015 [39] | 2,545 | / | 73.40 | 82.20 | / | / | / |
| Hua et al., 2015 [14] | 2,545 | / | 73.30 | 78.70 | / | / | / |
| Dhara et al., 2016 [8] | 1,945 | 87.90 | 84.50 | 89.09 | 93.77 | / | / |
| Song et al., 2017 [40] | 5,024 | 84.15 | 83.96 | 84.32 | / | / | / |
| Xie et al., 2018 [17] | 2,669 | 89.53 | 84.19 | 92.02 | 96.65 | 28,800 | 400 |
| Xie et al., 2019 [19] | 3,784 | 92.53 | 84.94 | 96.28 | 95.81 | 86,400 | 500 |
| Proposed Method | 2,757 | 94.57 | 93.69 | 95.15 | 94.94 | 1.72 | 0.5 |

4.3. Lung Nodule diagnosis with FAH-GMU

4.3.1. FAH-GMU dataset description

FAH-GMU dataset contained 115 patients of pulmonary consolidation who were confirmed at FAH-GMU between 2016 and 2019 with pathology and had at least one CT scan. There are sixty-eight patients with malignant pulmonary lesion and forty-seven patients with benign pulmonary lesion in the FAH-GMU dataset. The CT scan images with 2 mm slice thickness were attained and the location of nodules was recognized by at least two radiologists also provided in the dataset. Pulmonary lesions of the FAH-GMU dataset are shown in Fig. 6.



(a) benign pulmonary lesions in FAH-GMU (b) malignant pulmonary lesions in FAH-GMU

Fig. 6. Raw examples of (a) benign pulmonary lesions and (b) malignant pulmonary lesions in the FAH-GMU dataset.

4.3.2. FAH-GMU Training Details

Different from LIDC-IDRI, the FAH-GMU only contains 115 samples. Therefore, during the training process, Adam is applied for optimization with batches of size 4, the initial learning rate is set as 0.002 and decreases every 4 epochs with the factor of learning rate decay 0.5. The total number of training epoch is set as 20 in FAH-GMU experiments. The number of hidden nodes l in ELM is set as 50. Unless otherwise stated, all experiments are conducted 10 times in leave-one-out cross-validation.

4.3.3. The efficiency and effectiveness of DTCNN-ELM on FAH-GMU

The purpose of this experiment was to validate the efficiency and effectiveness of DTCNN-ELM on FAH-GMU dataset. The ResNet-50, Xception, NASNetMobile, MobileNetV2, and EfficientNet-B5 are compared with Softmax and ELM classifiers. The results of different combinations with DTCNN and classifier on the FAH-GMU dataset are reported in Table 5. As referred in Table 5, ResNet-50 with ELM has the best performance, with an Acc of 100%, a Sen of 100%, a Spc of 100%, and an AUC of 100%. Also, the training and testing time of ResNet-50 with ELM are 0.89s and 0.013s, respectively. However, not all DTCNN with ELM have superior classification results compared with those of softmax classifiers, such as MobileNetV2 and EfficientNet-B5. It is because such DTCNN has unreasonable structure or redundant parameters. In a word, DTCNN-ELM can effectively reduce computation costs and improve classification performance when the structure and parameters of DTCNN are suitable for datasets.

Table 5 Classification results and computation costs of different combinations with DTCNN and classifier.

| DTCNN | Classifier | Results (Mean) | | | | | |
|-----------------|------------|----------------|------------|------------|------------|----------------------|---------------------|
| | | Acc (%) | Sen (%) | Spc (%) | AUC (%) | Training Time (s) | Testing Time (s) |
| ResNet-50 | Softmax | 100 | 100 | 100 | 100 | 34.54 | 0.044 |
| | ELM | 100 | 100 | 100 | 100 | 0.89 | 0.013 |
| Xception | Softmax | 87.51 | 87.51 | 87.51 | 87.51 | 27.36 | 0.009 |
| | ELM | 92.86 | 87.51 | 100 | 92.86 | 0.63 | 0.007 |
| NASNetMobile | Softmax | 100 | 100 | 100 | 100 | 105.89 | 0.023 |
| | ELM | 100 | 100 | 100 | 100 | 3.30 | 0.021 |
| MobileNetV2 | Softmax | 92.86 | 87.51 | 100 | 92.86 | 25.48 | 0.006 |
| | ELM | 87.51 | 71.43 | 100 | 85.71 | 0.68 | 0.006 |
| EfficientNet-B5 | Softmax | 85.71 | 71.43 | 100 | 85.71 | 93.34 | 0.021 |
| | ELM | 71.43 | 71.43 | 71.43 | 71.43 | 3.13 | 0.019 |

5. Conclusions and future work

In this study, a novel method combining DTCNN and ELM is proposed towards fast and accurate automatically nodules benign–malignant diagnosis of the lung on CT images. DTCNN has shown a powerful high-feature extraction ability while ELM has been proposed to be an efficient and powerful classifier. Firstly, an optimal DTCNN is constructed by deep transfer learning and GAP, which is employed as an automatic feature extractor to enhance the feature learning capability. Secondly, the ELM is further applied to improve the classification performance and the learning speed. Finally, the proposed DTCNN-ELM method has been validated for recognizing nodules on the LIDC-IDRI public dataset and FAH-GMU private dataset. Experimental results suggest that combining the DTCNN with ELM can not only improves the classification performance of benign–malignant nodules but also effectively reduces the computational costs. The proposed DTCNN-ELM method achieves the accuracy of 94.57% on the LIDC-IDRI dataset and the accuracy of 100% on the FAH-GMU dataset. In our future work, we will focus on investigating different transfer learning schemes and ELM structures, aiming to make the proposed DTCNN-ELM model more robust and more accurate.

Acknowledgments

This research has been supported by the National Natural Science Foundation of China (NSFC) under Grant No. 51805179, No. 51721092, and the Fundamental Research Funds for the Central Universities, HUST: Grant No. 2016YXMS272.

References

- [1] R.L. Siegel, K.D. Miller, A. Jemal, Cancer statistics, 2019, CA: A Cancer Journal for Clinicians, 69 (2019) 7-34.
- [2] W.L. Bi, A. Hosny, M.B. Schabath, M.L. Giger, N.J. Birkbak, A. Mehrtash, T. Allison, O. Arnaout, C. Abbosh, I.F. Dunn, R.H. Mak, R.M. Tamimi, C.M. Tempany, C. Swanton, U. Hoffmann, L.H. Schwartz, R.J. Gillies, R.Y. Huang, H. Aerts, Artificial intelligence in cancer imaging: Clinical challenges and applications, CA Cancer J Clin, 69 (2019) 127-157.
- [3] X. Xu, C. Wang, J. Guo, L. Yang, H. Bai, W. Li, Z. Yi, DeepLN: A framework for automatic lung nodule detection using multi-resolution CT screening images, KNOWL-BASED SYST, (2019) 105128.
- [4] D.S. Kermany, M. Goldbaum, W. Cai, C.C.S. Valentim, H. Liang, S.L. Baxter, A. McKeown, G. Yang, X. Wu,

F. Yan, J. Dong, M.K. Prasadha, J. Pei, M.Y.L. Ting, J. Zhu, C. Li, S. Hewett, J. Dong, I. Ziyar, A. Shi, R. Zhang, L. Zheng, R. Hou, W. Shi, X. Fu, Y. Duan, V.A.N. Huu, C. Wen, E.D. Zhang, C.L. Zhang, O. Li, X. Wang, M.A. Singer, X. Sun, J. Xu, A. Tafreshi, M.A. Lewis, H. Xia, K. Zhang, Identifying Medical Diagnoses and Treatable Diseases by Image-Based Deep Learning, *CELL*, 172 (2018) 1122-1131.e9.

[5] M. Bari, A. Ahmed, S. Naveed, Lungs Cancer Detection Using Digital Image Processing Techniques: A Review, *Mehran University Research Journal of Engineering and Technology*, 38 (2019) 351-360.

[6] P. Grossmann, O. Stringfield, N. El-Hachem, M.M. Bui, V.E. Rios, C. Parmar, R.T. Leijenaar, B. Haibe-Kains, P. Lambin, R.J. Gillies, H.J. Aerts, Defining the biological basis of radiomic phenotypes in lung cancer, *ELIFE*, 6 (2017).

[7] F. Han, H. Wang, G. Zhang, H. Han, B. Song, L. Li, W. Moore, H. Lu, H. Zhao, Z. Liang, Texture Feature Analysis for Computer-Aided Diagnosis on Pulmonary Nodules, *J DIGIT IMAGING*, 28 (2015) 99-115.

[8] A.K. Dhara, S. Mukhopadhyay, A. Dutta, M. Garg, N. Khandelwal, A Combination of Shape and Texture Features for Classification of Pulmonary Nodules in Lung CT Images, *J DIGIT IMAGING*, 29 (2016) 466-475.

[9] V.E. Rios, C. Parmar, Y. Liu, T.P. Coroller, G. Cruz, O. Stringfield, Z. Ye, M. Makrigiorgos, F. Fennessy, R.H. Mak, R. Gillies, J. Quackenbush, H. Aerts, Somatic Mutations Drive Distinct Imaging Phenotypes in Lung Cancer, *CANCER RES*, 77 (2017) 3922-3930.

[10] N. Tajbakhsh, K. Suzuki, Comparing two classes of end-to-end machine-learning models in lung nodule detection and classification: MTANNs vs. CNNs, *PATTERN RECOGN*, 63 (2017) 476-486.

[11] G. Wei, H. Ma, W. Qian, F. Han, H. Jiang, S. Qi, M. Qiu, Lung nodule classification using local kernel regression models with out-of-sample extension, *BIOMED SIGNAL PROCES*, 40 (2018) 1-9.

[12] G. Litjens, T. Kooi, B.E. Bejnordi, A.A.A. Setio, F. Ciompi, M. Ghafoorian, J.A.W.M. van der Laak, B. van Ginneken, C.I. Sánchez, A survey on deep learning in medical image analysis, *MED IMAGE ANAL*, 42 (2017) 60-88.

[13] S. Napel, W. Mu, B.V. Jardim Perassi, H.J.W.L. Aerts, R.J. Gillies, Quantitative imaging of cancer in the postgenomic era: Radio(geno)mics, deep learning, and habitats, *CANCER-AM CANCER SOC*, 124 (2018) 4633-4649.

[14] K. Hua, C. Hsu, S.C. Hidayati, W. Cheng, Y. Chen, Computer-aided classification of lung nodules on computed tomography images via deep learning technique, *ONCOTARGETS THER*, 8 (2015).

[15] S.G. Armato, G. McLennan, L. Bidaut, M.F. McNitt-Gray, C.R. Meyer, A.P. Reeves, B. Zhao, D.R. Aberle, C.I. Henschke, E.A. Hoffman, E.A. Kazerooni, H. MacMahon, E.J.R. van Beek, D. Yankelevitz, A.M. Biancardi, P.H. Bland, M.S. Brown, R.M. Engelmann, G.E. Laderach, D. Max, R.C. Pais, D.P.Y. Qing, R.Y. Roberts, A.R. Smith, A. Starkey, P. Batra, P. Caligiuri, A. Farooqi, G.W. Gladish, C.M. Jude, R.F. Munden, I. Petkovska, L.E. Quint, L.H. Schwartz, B. Sundaram, L.E. Dodd, C. Fenimore, D. Gur, N. Petrick, J. Freymann, J. Kirby, B. Hughes, A. Vande Castele, S. Gupte, M. Sallam, M.D. Heath, M.H. Kuhn, E. Dharaiya, R. Burns, D.S. Fryd, M. Salganicoff, V. Anand, U. Shreter, S. Vastagh, B.Y. Croft, L.P. Clarke, The Lung Image Database Consortium (LIDC) and Image Database Resource Initiative (IDRI): A Completed Reference Database of Lung Nodules on CT Scans, *MED PHYS*, 38 (2011) 915-931.

[16] K. Clark, B. Vendt, K. Smith, J. Freymann, J. Kirby, P. Koppel, S. Moore, S. Phillips, D. Maffitt, M. Pringle, L. Tarbox, F. Prior, The Cancer Imaging Archive (TCIA): Maintaining and Operating a Public Information Repository, *J DIGIT IMAGING*, 26 (2013) 1045-1057.

[17] Y. Xie, J. Zhang, Y. Xia, M. Fulham, Y. Zhang, Fusing texture, shape and deep model-learned information at decision level for automated classification of lung nodules on chest CT, *INFORM FUSION*, 42 (2018) 102-110.

- [18] S.K. Lakshmanaprabu, S.N. Mohanty, S. K., A. N., G. Ramirez, Optimal deep learning model for classification of lung cancer on CT images, *Future Generation Computer Systems*, 92 (2019) 374-382.
- [19] Y. Xie, J. Zhang, Y. Xia, Semi-supervised adversarial model for benign – malignant lung nodule classification on chest CT, *MED IMAGE ANAL*, 57 (2019) 237-248.
- [20] Q. Wang, X. Zhou, C. Wang, Z. Liu, J. Huang, Y. Zhou, C. Li, H. Zhuang, J. Cheng, WGAN-Based Synthetic Minority Over-Sampling Technique: Improving Semantic Fine-Grained Classification for Lung Nodules in CT Images, *IEEE ACCESS*, 7 (2019) 18450-18463.
- [21] Q. Song, L. Zhao, X. Luo, X. Dou, Using Deep Learning for Classification of Lung Nodules on Computed Tomography Images, *J HEALTHC ENG*, 2017 (2017) 1-7.
- [22] W. Shen, M. Zhou, F. Yang, C. Yang, J. Tian, Multi-scale convolutional neural networks for lung nodule classification, *International Conference on Information Processing in Medical Imaging*, Springer, 2015, pp. 588-599.
- [23] D. Kumar, A. Wong, D.A. Clausi, Lung nodule classification using deep features in CT images, 2015 12th Conference on Computer and Robot Vision, IEEE, 2015, pp. 133-138.
- [24] R.V.M. Da Nóbrega, S.A. Peixoto, S.P.P. Da Silva, P.P. Rebouças Filho, Lung Nodule Classification via Deep Transfer Learning in CT Lung Images, 2018 IEEE 31st International Symposium on Computer-Based Medical Systems (CBMS), IEEE, 2018, pp. 244-249.
- [25] G. Xu, X. Shen, S. Chen, Y. Zong, C. Zhang, H. Yue, M. Liu, F. Chen, W. Che, A Deep Transfer Convolutional Neural Network Framework for EEG Signal Classification, *IEEE ACCESS*, 7 (2019) 112767-112776.
- [26] N. Tajbakhsh, J.Y. Shin, S.R. Gurudu, R.T. Hurst, C.B. Kendall, M.B. Gotway, J. Liang, Convolutional Neural Networks for Medical Image Analysis: Full Training or Fine Tuning? *IEEE T MED IMAGING*, 35 (2016) 1299-1312.
- [27] H.C. Shin, H.R. Roth, M. Gao, L. Lu, Z. Xu, I. Nogues, J. Yao, D. Mollura, R.M. Summers, Deep Convolutional Neural Networks for Computer-Aided Detection: CNN Architectures, Dataset Characteristics and Transfer Learning, *IEEE Trans Med Imaging*, 35 (2016) 1285-98.
- [28] Y. Xu, A. Hosny, R. Zeleznik, C. Parmar, T. Coroller, I. Franco, R.H. Mak, H.J.W.L. Aerts, Deep Learning Predicts Lung Cancer Treatment Response from Serial Medical Imaging, *CLIN CANCER RES*, (2019).
- [29] A. Krizhevsky, I. Sutskever, G.E. Hinton, Imagenet classification with deep convolutional neural networks, *Advances in neural information processing systems*, 2012, pp. 1097-1105.
- [30] Z. Kang, B. Yang, Z. Li, P. Wang, OTLAMC: An Online Transfer Learning Algorithm for Multi-class Classification, *KNOWL-BASED SYST*, 176 (2019) 133-146.
- [31] Y. LeCun, L. Bottou, Y. Bengio, P. Haffner, Gradient-based learning applied to document recognition, *P IEEE*, 86 (1998) 2278-2324.
- [32] G. Huang, Q. Zhu, C. Siew, Extreme learning machine: Theory and applications, *NEUROCOMPUTING*, 70 (2006) 489-501.
- [33] G. Huang, G.B. Huang, S. Song, K. You, Trends in extreme learning machines: a review, *Neural Netw*, 61 (2015) 32-48.
- [34] A.M. Anter, Y.S. Moemen, A. Darwish, A.E. Hassanien, Multi-target QSAR modelling of chemo-genomic data analysis based on Extreme Learning Machine, *KNOWL-BASED SYST*, (2019) 104977.
- [35] S. Balasundaram, D. Gupta, Kapil, 1-Norm extreme learning machine for regression and multiclass classification using Newton method, *NEUROCOMPUTING*, 128 (2014) 4-14.
- [36] M. Wang, W. Deng, Deep visual domain adaptation: A survey, *NEUROCOMPUTING*, 312 (2018) 135-153.
- [37] C. Tan, F. Sun, T. Kong, W. Zhang, C. Yang, C. Liu, A survey on deep transfer learning, *International Conference on Artificial Neural Networks*, Springer, 2018, pp. 270-279.

- [38] M. Lin, Q. Chen, S. Yan, Network in network, arXiv preprint arXiv:1312.4400, (2013).
- [39] Y. Yu-Jen Chen, K. Hua, C. Hsu, W. Cheng, S.C. Hidayati, Computer-aided classification of lung nodules on computed tomography images via deep learning technique, ONCOTARGETS THER, 2015.
- [40] Q. Song, L. Zhao, X. Luo, X. Dou, Using deep learning for classification of lung nodules on computed tomography images, J HEALTHC ENG, 2017 (2017).